POLITECNICO DI TORINO
Repository ISTITUZIONALE

Spherical voids by finite fracture mechanics

Original
Spherical voids by finite fracture mechanics / Chao Correas, A., Corrado, M., Sapora, A., Cornetti, P.. - In: PROCEDIA STRUCTURAL INTEGRITY. - ISSN 2452-3216. - 33:(2021), pp. 788-794. (26th International Conference on Fracture and Structural Integrity, IGF26 2021 Torino, Italy 26-31/05/2021) [10.1016/j.prostr.2021.10.087].

Availability:
This version is available at: 11583/2959392 since: 2023-01-27T10:03:58Z

Publisher:
Elsevier

Published
DOI:10.1016/j.prostr.2021.10.087

Terms of use:

This article is made available under terms and conditions as specified in the corresponding bibliographic description in the repository

Publisher copyright

(Article begins on next page)

29 November 2026

Available online at www.sciencedirect.com

ScienceDirect

Procedia Structural Integrity 33 (2021) 788–794

Structural Integrity Procedia

www.elsevier.com/locate/procedia

IGF26 - 26th International Conference on Fracture and Structural Integrity

Spherical voids by finite fracture mechanics

A. Chao Correas*, M. Corrado, A. Sapora, P. Cornetti

Department of Structural, Building and Geotechnical Engineering, Politecnico di Torino, Corso Duca degli Abruzzi 24, 10129, Torino, Italy

Abstract

The apparent weakening of a uniaxially tensioned infinite domain that contains a single spherical void and is anywhere else filled with a homogeneous and linear elastic material is investigated through two Finite Fracture Mechanics approaches. Resultant charts depicting the respectively predicted relation of the weakening ratio with the void's radius clearly show that the fracture toughness drives the transition between the strength-dominated extreme solutions, namely voidless and large void. Eventually, the Finite Fracture Mechanics predictions are compared with experimental results, yielding a reasonably good agreement.

© 2021 The Authors. Published by Elsevier B.V.
This is an open access article under the CC BY-NC-ND license (https://creativecommons.org/licenses/by-nc-nd/4.0)
Peer-review under responsibility of the scientific committee of the IGF ExCo

Keywords: Fracture mechanics; spherical cavity; size effect; brittle materials.

1. Introduction

The presence of defects causing stress concentrations within structural components leads to a reduction of their apparent strength in comparison with pristine conditions, as highlighted in Taylor et al. (2009) for the case of human bones. However, this weakening's magnitude has a strong dependence on the geometrical characteristics of the flaw itself, namely its shape and size. Hence, since spherical-like pores are relatively common features in structural components due to manufacturing deviations, the decrease in the strength of infinite domains under uniaxial tensile conditions and containing a single spherical void will be studied in this work. For the sake of simplicity, the material behavior hereafter considered will always be linear elastic and brittle. Particular attention will also be paid to the so-called size-effect, i.e. the dependence of the weakening magnitude with the size of self-like geometrical features.

* Corresponding author. Tel.: +39 011 090 5312; fax: +39 011 090 4899.
E-mail address: arturo.chaocorreas@polito.it

2452-3216 © 2021 The Authors. Published by Elsevier B.V.
This is an open access article under the CC BY-NC-ND license (https://creativecommons.org/licenses/by-nc-nd/4.0)
Peer-review under responsibility of the scientific committee of the IGF ExCo
10.1016/j.prostr.2021.10.087

In this regard, different pieces of research have already studied the effect of spherical voids on the apparent strength of specimens. Experiments on samples with variable porosity and pore sizes were conducted by Bertolotti and Fulrath (1967) on borosilicate glass and by Zhao et al. (2017) for alumina composites. These results showed that even very low porosities may lead to a significant reduction of the apparent strength. Likewise, the extent of weakening was found to be highly dependent on the pore size. On the other hand, relevant theoretical analyses on the topic were performed by Evans et al. (1979) on the basis of the Weibull statistic framework, and by Krstic (1985, 2006) through the implementation of LEFM approaches under the assumption of the ever-presence of an annular crack.

However, to the authors' best knowledge, no previous study has ever faced the implementation of Finite Fracture Mechanics (FFM) in the mentioned scenario. This theoretical tool, which was first proposed by Leguillon (2002) and then partially modified by Cornetti et al. (2006), has already been successfully applied for several both singular and non-singular geometries, including slabs with through-the-thickness cracks by Cornetti et al. (2016) and Sapora et al. (2020); penny-shaped cracks by Cornetti and Sapora (2019); plates with circular holes by Leguillon and Piat (2008), Camanho et al. (2012), Martin et al. (2012) and Sapora and Cornetti (2018); or notched specimens under bending by Cornetti et al. (2006) and Doitrand et al. (2021).

Hereafter, the implementation of FFM for spherical voids is presented. To that end, the required input functions, i.e. the uncracked stress field and the annular crack Stress Intensity Factor (SIF), are provided in Section 2. As of these expressions, the particularization of the two main FFM variants is presented in Section 3, followed then by a comparison with experimental data in Section 4. Eventually, the final conclusions are drawn in Section 5.

2. The annular crack around a spherical void

Let us consider an infinite domain filled with a homogeneous, linear elastic and brittle material that is subjected to uniaxial tensile conditions and contains a single spherical pore within, as represented in Fig. 1a). Under these conditions, the stress concentration is maximum in the void's equator, and so, failure is expected to nucleate as a mode I crack contained within the $z = 0$ plane. Moreover, on such a plane, and prior to any crack propagation, the normal stress component σ_{zz} is defined by the Eq. (1) according to Goodier (1933). This exact analytical expression implies that the stress concentration directly depends on the Poisson's ratio ν, being this a particularity of the geometry at hand. In this work, ν will be always taken as 0.2, which results in a stress concentration K_T equal to 2.0.

$$\sigma_{zz}\left(r,\theta,0\right)=\sigma_{\infty}\left[1+\frac{4-5\nu}{14-10\nu}\left(\frac{R}{r}\right)^{3}+\frac{9}{14-10\nu}\left(\frac{R}{r}\right)^{5}\right] \tag{1}$$

Since there is no dependence with θ of the material properties, the geometry and the stress field, the problem is treated as axisymmetric. This consideration also concerns the crack propagation pattern, which is assumed to take place as an annular crack surrounding the void's equator, as shown in Fig. 1b).

Besides, an approximate definition of the SIF of an annular crack of radial length a surrounding the spherical void of radius R was given by Fett (1994), whose proposal was based on the assumption that the annular crack resembles a penny-shaped crack in the limit $a >> R$. Thus, this approximation of the SIF of an annular crack was built onto that of a penny-crack of radius $R + a$, loaded according to Eq. (1) in the range $r \in [R, R + a]$. A proper correction factor was added for also complying with the limit case for $R >> a$, which would be that of an edge crack under constant stress equal to the void's stress concentration, i.e. $(K_T \cdot \sigma_{\infty})$. This resultant SIF expression derived by Fett (1994) is provided in Eqs. (2) and (3).

$$K_I^{\sigma_{\infty}}=\sigma_{\infty}\sqrt{\pi a}F^{\sigma_{\infty}}(a,R) \tag{2}$$

$$F^{\sigma_{\infty}}(a,R)=\frac{2}{\pi}\sqrt{\frac{a+2R}{a+R}}\left[1+\frac{R^2}{2\left(R+a\right)^2}+\frac{3R^4}{\left(7-5\nu\right)\left(R+a\right)^4}\right]+\frac{9-5\nu}{21-15\nu}\frac{R^2}{\left(R+2a\right)^2} \tag{3}$$

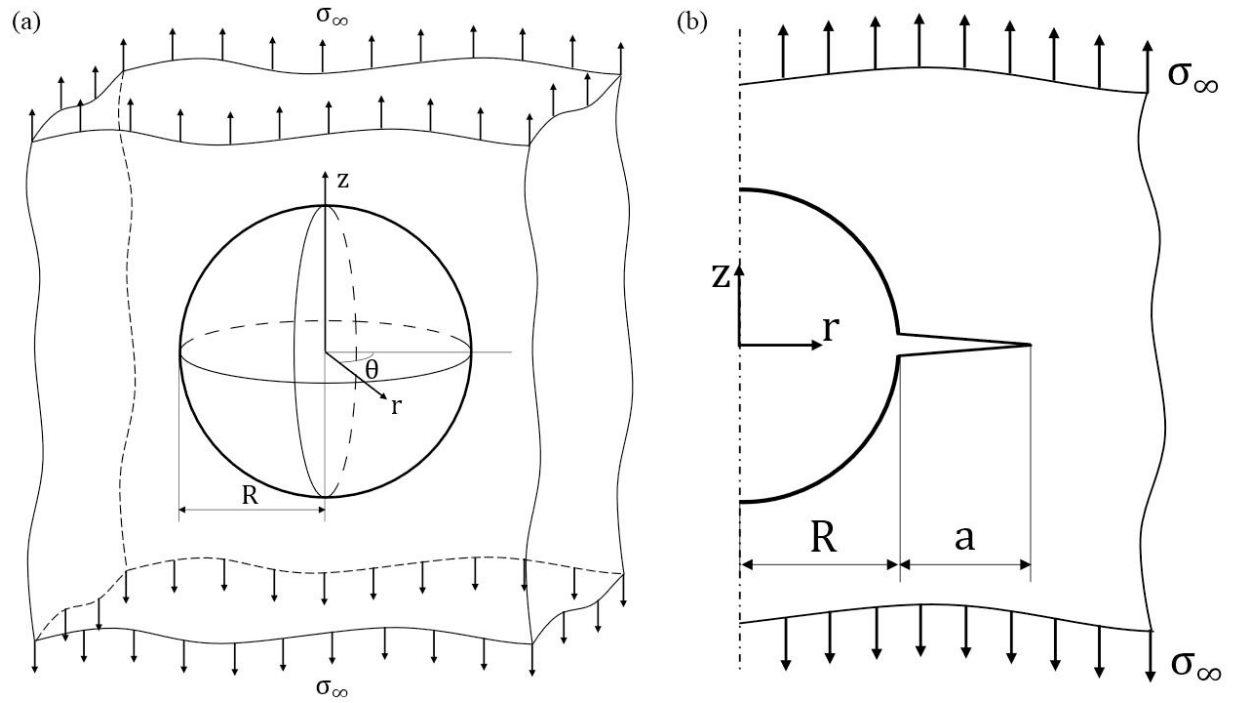


Fig. 1. Schematic representation of: (a) a spherical void in an infinite tensioned body in 3D, (b) axisymmetric reduction of the problem.

3. Finite Fracture Mechanics

The FFM failure criterion consists in considering that crack propagation occurs spontaneously and in a finite manner upon the simultaneous fulfilment of certain energetic and stress conditions. The specifics of each of these conditions depend on the variant considered. Likewise, the resultant failure state comes characterized by a failure load σ_f, which represents the lowest externally applied stress σ_∞ that allows the fulfilment of both necessary failure conditions, plus a finite length Δ that represents the characteristic distance over which the crack suddenly propagates upon reaching the failure state. Therefore, to obtain a failure prediction by means of FFM it is generally required to solve a nonlinearly conditioned minimization problem. Nonetheless, since the considered geometry is positive, i.e. $\partial G / \partial a > 0$, and the relevant component of the stress field is monotonically decreasing with respect to r all along the prospective crack plane, the resolution of the problem is simplified to that of a system of two nonlinear equations with two unknowns.

Moreover, since no plasticity is considered in the material behaviour, the crack resistance is independent of the crack length. Added this to the positiveness of the geometry, no stable crack propagation can happen after crack initiation. Therefore, crack onset and complete failure coincide for the given scenario.

3.1. Original formulation

The original FFM formulation was proposed by Leguillon (2002), where it was introduced as a coupled energetic/stress failure criterion. Concerning the stress condition, it is imposed that all along the region over which the crack would subsequently propagate, the crack opening stress σ_{zz} should be higher than the critical stress σ_c, i.e. $\sigma_{zz}(r, \theta, 0) \geq \sigma_c, \forall\, r \in \{r \mid R \leq r \leq R + \Delta\}$. Nonetheless, this is simplified to Eq. (4a) for monotonically decreasing stress fields. On the other hand, the energetic condition requires the energy available for crack propagation to be equal

to or higher than the energy required for creating that new surface. By using now the Irwin's relation, this requirement can be written in terms of the SIF and fracture toughness K_{Ic} as in Eq. (4b).

$$\sigma_{zz}(R+\Delta)\geq\sigma_c \tag{4a}$$

$$\int_0^{\Delta} 2\pi(a+R)\left(K_I^{\sigma_\infty}(a)\right)^2 da\geq\pi\left[(R+\Delta)^2-R^2\right]K_{Ic}^{\ 2} \tag{4b}$$

As already stated, the positiveness of the geometry simplifies the FFM implementation to a nonlinear system of two equations with two unknowns. Introducing the stress field and SIF from Eqs. (1), (2) and (3), as well as Irwin's length $l_{ch}=(K_{Ic}/\sigma_c)^2$, the development of Eqs. (4a) and (4b) results in Eqs. (5a) and (5b). The resolution of the integral in Eq. (5b), as well as that of the complete system of equations in Eqs. (5a) and (5b) is to be performed numerically.

$$\frac{\sigma_f}{\sigma_c}=\left[1+\frac{4-5\nu}{14-10\nu}\left(\frac{R}{R+\Delta}\right)^3+\frac{9}{14-10\nu}\left(\frac{R}{R+\Delta}\right)^5\right]^{-1} \tag{5a}$$

$$\frac{\sigma_f}{\sigma_c}=\sqrt{\frac{l_{ch}\left(\Delta^2+2\Delta R\right)}{2\pi\int_0^{\Delta} a\left(F^{\sigma_\infty}(a)\right)^2(a+R)da}} \tag{5b}$$

3.2. Averaged stress formulation

The FFM reformulation proposed by Cornetti et al. (2006) (FFM-avg) only modified the stress condition. In that work, the authors required that the resultant force of the relevant stress component for failure, calculated over the area in which the crack would subsequently propagate, should be equal to or larger than the critical stress times that very same area. Mathematically, this is shown in Eq. (6).

$$\int_0^{\Delta} 2\pi r\left(\sigma_{zz}(r)\right)dr\geq\pi\left[(R+\Delta)^2-R^2\right]\sigma_c \tag{6}$$

Introducing the stress field in Eq. (1) into the generalized stress condition in Eq. (6), results in the FFM averaged stress (FFM-avg) stress condition of failure in Eq. (7), while the respective energetic condition remains as in Eq. (5b).

$$\frac{\sigma_f}{\sigma_c}=\frac{\Delta^2+2\Delta R}{\Delta^2+2\Delta R-\frac{4+5\nu}{7-5\nu}\left(\frac{R^3}{R+\Delta}-R^2\right)-\frac{3}{7-5\nu}\left(\frac{R^5}{(R+\Delta)^3}-R^2\right)} \tag{7}$$

The charts containing the predictions by both FFM formulations for the weakening ratio σ_f/σ_c as a function of the void radius are shown in Fig. 2a). As seen, both variants can capture, although differently, the transition between extreme cases, i.e. from the voidless ($\sigma_f/\sigma_c = 1$) to the large void ($\sigma_f/\sigma_c = 1/K_T$) solutions. Besides, just as it was noticed for other geometries, FFM-avg provides more conservative failure predictions than FFM.

With respect to the relation of the finite crack extension Δ with the void radius, shown in Fig. 2b), both FFM formulations coincide at the extreme solutions, yielding the figures $3l_{ch}\pi/8$ for $R\rightarrow 0$ and $2l_{ch}/1.122^2\pi$ for $R\rightarrow\infty$. In turn, these results coincide with the finite crack extensions reported in the literature for Penny-shaped cracks in Cornetti and Sapora (2019) and for Edge cracks in Cornetti et al. (2006), being also coherent with the collapse of the

analysed geometry to these two simpler cases, as stated in Section 2. Eventually, it is also seen that the finite crack extension predicted by FFM presents smaller finite crack propagations and a much more abrupt transition in comparison with that of FFM-avg.

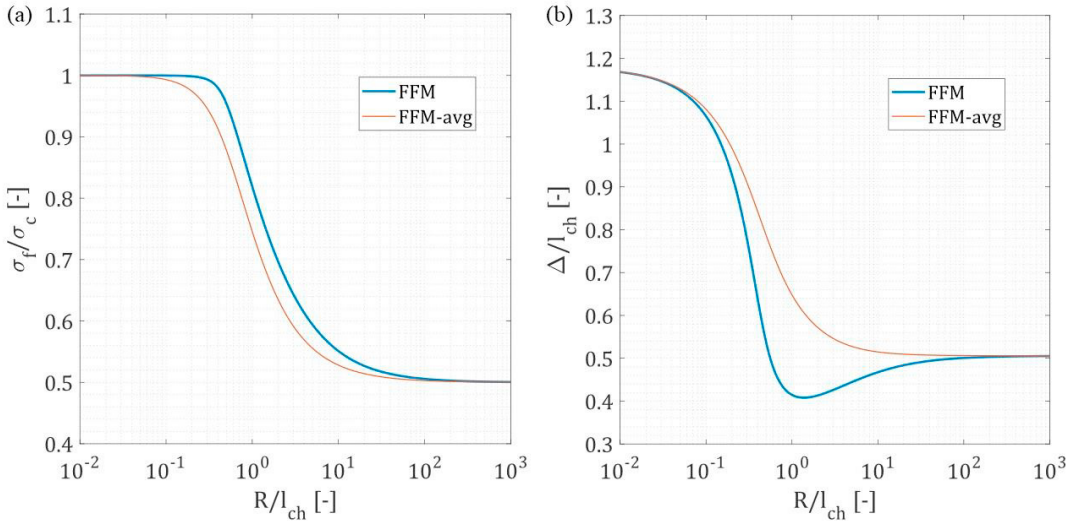


Fig. 2. Comparison of FFM and FFM-avg predictions for: (a) weakening ratio; (b) finite crack extensions.

4. Comparison with experimental data

Within this section, the accuracy of the weakening predictions delivered by each FFM approach is checked by means of comparison against the experimental results by Bertolotti and Fulrath (1967). For this experimental campaign, sodium borosilicate specimens with controlled porosity and pore size were manufactured. Given the high brittleness of sodium borosilicate, which causes the failure to be flaw-governed, the specimens had a surface treatment that ensured that the critical flaw size was between 12.9 to 26.5 microns in length in an aim to reduce the experimental scatter. The average value of these two limit dimensions (times π) is taken as the structural l_{ch} for the undertaken comparison.

Thereafter, the local tensile conditions were generated by a four-point bending setup. Then, the apparent strength was calculated out of the registered peak load and compared against the figure obtained to that from non-porous self-like specimens. Nonetheless, due to the random location of the pores with respect to either the free surface, the surface flaws and other pores, experimental scatter in the vertical axis was still expected. On the other hand, the uncertainty in the critical pore size was, in turn, found responsible for the scatter in the horizontal axis.

Eventually, since the present work only concerns single void conditions, solely the two lowest porosity cases from the reference are considered for the comparison in Fig. 3. Therein, the experimental uncertainty is dealt with through the obtention of the 95% confidence intervals for each set of results. The steep drop in the apparent strength in the surroundings of $R \sim l_{ch}$ for the 5% porosity case infers that non-negligible pore interaction takes place, thus making these sets of results less representative for comparison purposes. As a result, by only considering the lowest porosity case (2%), it is clear that FFM-avg not only provides accurate predictions with respect to experimental data but also reduces the error in comparison with those from FFM.

5. Conclusions

The weakening caused by a spherical void within a structural domain filled with a linear elastic and brittle material and subjected to uniaxially tension conditions is investigated in this study. Despite not being a singular geometry, the resultant localized stress concentration precludes the use of the maximum stress criterion and requires accounting for

energetic quantities to capture the so-called size effect. Thus, the implementation of the two FFM variants is undertaken in this study, making use of stress field and SIF expressions available in the literature. Despite the differences, both can catch properly the transition between extreme solutions, although FFM-avg is more accurate with respect to relevant experimental results.

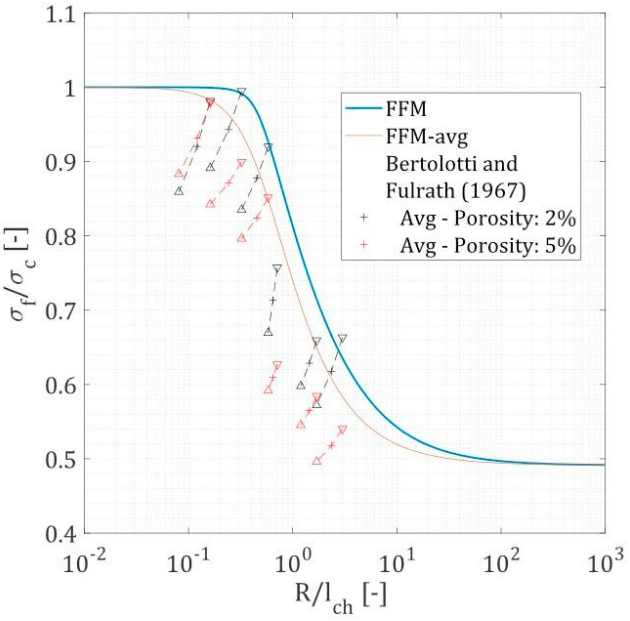


Fig. 3. Comparison of the failure predictions of FFM and FFM-avg with respect to experimental results by Bertolotti and Fulrath (1967)

Acknowledgements

The funding received from the European Union's Horizon 2020 research and innovation program under Marie Skłodowska-Curie grant agreement No. 861061-NEWFRAC is gratefully acknowledged.

References

Bertolotti, R. L., Fulrath, R. M., 1967. Effect of Micromechanical Stress Concentrations on Strength of Porous Glass. Journal of the American Ceramic Society 50, 558–562. https://doi.org/10.1111/j.1151-2916.1967.tb14998.x

Camanho, P. P., Erçin, G. H., Catalanotti, G., et al, 2012. A finite fracture mechanics model for the prediction of the open-hole strength of composite laminates, Composites Part A: Applied Science and Manufacturing 43, 1219–1225. https://doi.org/10.1016/j.compositesa.2012.03.004

Cornetti, P., Pugno, N., Carpinteri, A., Taylor, D., 2006. Finite fracture mechanics: A coupled stress and energy failure criterion. Engineering Fracture Mechanics 73, 2021–2033. https://doi.org/10.1016/j.engfracmech.2006.03.010

Cornetti, P., Sapora, A., 2019. Penny-shaped cracks by Finite Fracture Mechanics. International Journal of Fracture 219, 153–159. https://doi.org/10.1007/s10704-019-00383-9

Cornetti, P., Sapora, A., Carpinteri, A., 2016. Short cracks and V-notches: Finite Fracture Mechanics vs. Cohesive Crack Model. Engineering Fracture Mechanics 168, 2–12. https://doi.org/10.1016/j.engfracmech.2015.12.016

Doitrand, A., Henry, R., Meille, S., 2021. Brittle material strength and fracture toughness estimation from four-point bending test. Journal of Theoretical, Computational and Applied Mechanics, 1-17. https://doi.org/10.46298/jtcam.6753

Evans, A. G., Biswas, D. R., Fulrath, R. M., 1979. Some Effects of Cavities on the Fracture of Ceramics: II, Spherical Cavities. Journal of the American Ceramic Society 62, 101–106. https://doi.org/10.1111/j.1151-2916.1979.tb18815.x

Fett, T., 1994. Stress intensity factors and weight function for a void with an annular crack. International Journal of Fracture 67, 41–47. https://doi.org/10.1007/BF00019608

Goodier, J. N., 1933. Concentration of stress around spherical and cylindrical inclusions and flaws. Journal of Applied Mechanics 55, 39–44.

Krstic, V. D., 1985. Fracture of brittle solids in the presence of a spherical cavity. Acta Metallurgica 33, 521–526. https://doi.org/10.1016/0001-6160(85)90094-X

Krstic, V. D., 2006. Effect of microstructure on fracture of brittle materials: Unified approach. Theoretical and Applied Fracture Mechanics 45, 212–226. https://doi.org/10.1016/j.tafmec.2006.03.005

Leguillon, D., 2002. Strength or toughness? A criterion for crack onset at a notch. European Journal of Mechanics-A/Solids 21, 61–72. https://doi.org/10.1016/S0997-7538(01)01184-6

Leguillon, D., Piat, R., 2008. Fracture of porous materials-Influence of the pore size. Engineering Fracture Mechanics 75, 1840–1853. https://doi.org/10.1016/j.engfracmech.2006.12.002

Martin, E., Leguillon, D., Carrère, N., 2012. A coupled strength and toughness criterion for the prediction of the open hole tensile strength of a composite plate. International Journal of Solids and Structures 49, 3915–3922. https://doi.org/10.1016/j.ijsolstr.2012.08.020

Sapora, A., Cornetti, P., 2018. Crack onset and propagation stability from a circular hole under biaxial loading. International Journal of Fracture 214, 97–104. https://doi.org/10.1007/s10704-018-0315-6

Sapora, A., Cornetti, P., Campagnolo, A., Meneghetti, G., 2020. Fatigue limit: Crack and notch sensitivity by Finite Fracture Mechanics. Theoretical and Applied Fracture Mechanics 105, 102407. https://doi.org/10.1016/j.tafmec.2019.102407

Taylor, D., Kasiri, S. and Brazel, E., 2009. The theory of critical distances applied to problems in fracture and fatigue of bone, Frattura ed Integrità Strutturale 10, 12–20. https://doi.org/10.3221/IGF-ESIS.10.02.

Zhao, B., Yu, T., Ding, W., Li, X., 2017. Effects of pore structure and distribution on strength of porous Cu-Sn-Ti alumina composites. Chinese Journal of Aeronautics 30, 2004–2015. https://doi.org/10.1016/j.cja.2017.08.008